The broad spectrum mixed-lineage kinase 3 inhibitor URMC-099 prevents acute microgliosis and cognitive decline in a mouse model of perioperative neurocognitive disorders

Patrick Miller-Rhodes[1,2], Cuicui Kong[3], Gurpreet S. Baht[4], Ramona M. Rodriguiz[5], William C. Wetsel[5,6], Harris A. Gelbard[1,2,7,8]*, Niccolò Terrando[3]*

[1]Center for Neurotherapeutics Discovery, and [2]Department of Neuroscience, University of Rochester Medical Center, Rochester, NY 14642,

[3]Center for Translational Pain Medicine, Department of Anesthesiology, Duke University Medical Center, Durham, NC, 27710, USA

[4]Department of Orthopedic Surgery and Duke Molecular Physiology Institute, Duke University Medical Center, Durham, NC, 27710, USA,

[5]Department of Psychiatry and Behavioral Sciences, Mouse Behavioral and Neuroendocrine Analysis Core Facility, Duke University Medical Center, Durham, North Carolina 27710, USA,

[6]Departments of Neurobiology and Cell Biology, Duke University Medical Center, Durham, NC 27710 USA,

[7]Department of Neurology, [8]Departments of Pediatrics and Microbiology and Immunology, University of Rochester Medical Center, Rochester, NY 14642,

* shared correspondence: Harris_Gelbard@URMC.Rochester.edu; niccolo.terrando@duke.edu

Acknowledgments: We wish to thank Mr. Christopher Means of the Duke University Mouse Behavioral and Neuroendocrine Analyses Core Facility for his care of the animals and diligent work during behavioral testing; Dr. Ping Wang in the Terrando lab for helping with the CLARITY samples; and Monique Mendes in Ania Majewska's lab (URMC) for helping with the acquisition of the 2-photon microscopy data. Design, synthesis and validation of URMC-099 was supported, in part, by NIH grants P01MH64570 and RO1 MH104147 (HAG). URMC-099 is owned by URMC (HA Gelbard. lead inventor: patent nos. US 8,846,909 B2; 8,877,772; and 9,181,247 and associated international patents). HAG has no commercial disclosures regarding URMC-099 at present. The study was supported by the NIH RO1 AG057525 (NT).

Abstract

Perioperative neurocognitive disorders (PND), including delirium and postoperative cognitive dysfunction, are serious complications that afflict up to 50% of surgical patients and for which there are no disease-modifying therapeutic options. Here, we test whether prophylactic treatment with the broad spectrum mixed-lineage kinase 3 inhibitor URMC-099 prevents surgery-induced neuroinflammation and cognitive impairment in a translational model of orthopedic surgery-induced PND. We used a combination of two-photon scanning laser microscopy and CLARITY with light-sheet microscopy to define surgery-induced changes in microglial dynamics and morphology. Orthopedic surgery induced widespread microglial activation in the hippocampus and cortex that accompanied impairments in episodic memory. URMC-099 prophylaxis prevented these neuropathological sequelae without impacting bone fracture healing. Together, these findings provide compelling evidence for the advancement of URMC-099 as a therapeutic option for PND.

Introduction

Delirium and postoperative cognitive dysfunction, now collectively referred to as perioperative neurocognitive disorders (PND), have become the most common complications after routine surgical procedures (Ags/Nia Delirium Conference Writing Group & Faculty, 2015; Evered et al., 2018). Following surgery, such as common orthopedic procedures, up to 50% of patients experience cognitive disturbances, which can lead to serious complications including poorer prognosis and higher 1-year mortality in subjects with pre-existing neurodegeneration (Lee, Oldham, Sieber, & Oh, 2017). PNDs have profound effects on our society and are estimated to incur tens of billions of dollars in health care costs annually (Leslie, Marcantonio, Zhang, Leo-Summers, & Inouye, 2008). Currently, there are no safe disease-modifying therapeutic options to treat PNDs and the pathogenesis of these complex phenomena is not fully understood.

To clarify the pathophysiology of PNDs, we have developed an orthopedic surgery mouse model where the left hind limb is subjected to an open tibial fracture with intramedullary fixation under general anesthesia and analgesia (Xiong, Zhang, Baht, & Terrando, 2018). This recapitulates features of clinical procedures such as a fracture repair or hip arthroplasty, which often associate with neurological disorders in frail subjects. In this model, we and others have described a key role for surgery-induced neuroinflammation, including changes in microglial and astrocytes morphology, and hippocampal-dependent memory impairments using both electrophysiology and behavioral assays (Cibelli et al., 2010; Terrando et al., 2013; Terrando et al., 2010; Zhang et al., 2016). A role for microglia activation has been also suggested in patients after abdominal surgery developing long-lasting cognitive impairments using [^{11}C]PBR28 imaging (Forsberg et al., 2017). Notably, strategies aimed at depleting microglia before surgery abrogated neuroinflammation and subsequent cognitive decline in mice (Feng et al., 2017), though careful risk/benefit analyses are needed for translation into patients.

Using a variety of preclinical models of disease that feature neuroinflammation, including HIV-1-associated neurocognitive disorders (HAND) (Marker et al., 2013), Alzheimer's disease (AD) and multiple sclerosis (MS) (Bellizzi et al., 2018) we have demonstrated the therapeutic efficacy of the small-molecule, blood-brain barrier (BBB)-permeable, mixed-lineage kinase 3 (MLK3) inhibitor URMC-099 (Dong et al., 2016; Kiyota et al., 2018). In addition to exhibiting favorable pharmacokinetic and toxicity profiles in rodents, URMC-099 possesses "broad-spectrum" activity due to its ability to inhibit multiple kinases that mediate pathological interactions between innate immune cells and end-organ target cells (such as neurons) (Bellizzi et al., 2018; Marker et al., 2013). Although URMC-099 and other immuno-modulatory approaches can reduce harmful microglial response in a variety of chronic neuroinflammatory settings, they may pose translational concerns in the context of acute perioperative recovery, such as impairing normal healing and tissue regeneration after surgical trauma.

Here, we test the hypothesis that prophylactic URMC-099 treatment attenuates neuroinflammation and PND-like deficits using an established model of orthopedic surgery. Using a combination of longitudinal two-photon laser scanning microscopy (2P-LSM) and translationally relevant behavioral paradigms, we show that prophylactic URMC-099 treatment reduces pathological changes in microglial morphology while preventing memory decline. Finally, we observed no adverse effects of URMC-099 treatment on bone healing following orthopedic surgery.

Results and discussion

URMC-099 treatment reverses microgliosis and BBB leak following orthopedic surgery

Microgliosis and BBB opening accompany cognitive deficits in mice after orthopedic surgery (Cibelli et al., 2010; Terrando et al., 2011; Terrando et al., 2013; Terrando et al., 2010; Xiong et al., 2018). We first evaluated whether URMC-099 treatment could reverse these pathological changes in a cohort of 9-month old male mice. Mice were treated with three doses of URMC-099 (10 mg/kg) before surgery and two doses after surgery, with all dosing spaced 12 hours apart. We selected this dosing paradigm for our initial experiment because it effectively inhibited phosphorylation of whole brain c-Jun N-terminal kinase

(JNK), a kinase downstream of MLK3, in an *in vivo* model of HIV-1 associated neurocognitive disorders (Goodfellow et al., 2013). At 24 hours post-surgery, hippocampal microgliosis was observed in vehicle-treated mice receiving orthopedic surgery relative to sham-treated controls using stereological analysis of F4/80+ cells (**Figure 1a, b**). In contrast, URMC-099-treated mice exhibited a significant reduction ($p < 0.001$) in the density of F4/80+ cells in the hippocampus to sham-treated control levels (**Figure 1b**), indicating that our treatment paradigm effectively inhibited surgery-induced hippocampal microgliosis. BBB integrity was also measured using IgG immunostaining. We observed a significant reduction ($p = 0.017$) in IgG leak in URMC-099-treated mice receiving surgery when compared to vehicle-treated mice receiving the same manipulation (**Figure 1c**).

URMC-099 prophylaxis prevents microglial morphological changes following orthopedic surgery.

We next tested whether URMC-099 prophylaxis — pre-treatment with three doses of URMC-099 (10 mg/kg, i.p.) with the last dose occurring an hour before surgery — is sufficient to *prevent* microglial activation following orthopedic surgery. Because others have observed changes in microglial morphology and process motility following a systemic inflammatory stimulus (Gyoneva et al., 2014; Paris et al., 2018), we used two approaches to define surgery-induced changes in microglial physiology and to test URMC-099's ability to prevent such changes: (1) longitudinal 2-photon laser scanning microscopy (2PLSM) to define the morphology and dynamics of microglia in the superficial layers of somatosensory cortex, and (2) light-sheet microscopy of CLARITY-processed hippocampal sections to define global changes in microglial morphology in the hippocampus. Longitudinal 2PLSM was performed by imaging vehicle or URMC-099-treated mice immediately prior to and 24 hours post-orthopedic surgery and was achieved using a modified thin-skull cortical window (TSCW) technique (Clark, Mikofsky, Lawson, & Sulzer, 2018). Vehicle-treated mice exhibited a reduction in the process complexity of microglia post-surgery compared to pre-surgery images, as quantified by cell "sphericity", or the normalized ratio of a microglia's volume to its surface area (**Figure 2a, b**). Notably, URMC-099 prophylaxis abrogated this effect, as microglia from URMC-099-treated mice remained mostly unchanged between pre- and post-surgery images (**Figure 2a, b**). This finding was replicated on a more global scale using CLARITY (**Figure 2e, f**). We also evaluated microglial process motility using our longitudinal 2PLSM paradigm. However, we detected no significant differences in microglial process motility between pre- and post-surgery images irrespective of treatment (**Figure 2c, d**). Although others have observed increases in microglial process motility following intraperitoneal LPS injection (Gyoneva et al., 2014), this report is contradicted by other work demonstrating no changes (Kondo, Kohsaka, & Okabe, 2011) or decreased motility (Paris et al., 2018) under similar, albeit not identical, conditions. Thus, it is also possible that surgical trauma and peripheral LPS injection elicit distinct effects on microglial physiology by, for example, impinging on different innate-immune signaling pathways. In support of this notion, genetic knockout of *Tlr4* does not prevent cognitive decline in mice receiving orthopedic surgery (Terrando et al., 2010).

URMC-099 prophylaxis abrogates orthopedic surgery-induced memory deficits

We evaluated cognitive dysfunction in our orthopedic surgery model using two translationally relevant behavioral tasks that probe hippocampal-dependent memory: the "What-When-Where" task (DeVito & Eichenbaum, 2010) and the Memory Load Object Discrimination task (Sannino et al., 2012). We tested for cognitive impairment beginning 24 hours post-surgery; as such, our behavioral paradigm models acute, delirium-like cognitive deficits, similar to those observed in a prospective cohort study of elderly orthopedic surgical patients (Witlox et al., 2013). The "What-When-Where" task tests various components of episodic memory in mice by requiring mice to remember which objects they explored, object location, and when they explored different objects over a series of trials in which objects are moved and/or replaced (**Figure 3a**). Repeated measures ANOVA (RMANOVA) revealed a main effect of treatment [$F(3, 36) = 5.872$, $p = 0.0023$]. Pairwise comparisons between the vehicle-treated surgery group and other experimental conditions showed significant impairment in memory performance of the vehicle-treated surgery group relative to vehicle-treated and URMC-099-treated sham groups in both the "What" and "Where" aspects of the task (**Figure 3b**). Additionally, we found that URMC-099 completely prevented the surgery-induced memory impairment in the "Where" aspect ($p = 0.0072$) while marginally preventing

impairment in the “What” aspect ($p = 0.0473$) (**Figure 3b**). We did not detect any differences in performance between our experimental conditions in the “When” aspect of the task; however, this is likely due to poor performance observed in our sham control groups. We did detect a main effect of treatment on distance moved across the three trials of the “What-When-Where” task [$F (3, 108) = 13.56$, $p<0.0001$] (**Supplemental Figure 1b**). However, multiple comparisons revealed that for both vehicle- and URMC-099-treated groups, mice that received orthopedic surgery moved *more* than their sham counterparts during the first trial (“set A”) of the task (URMC099/Sham vs URMC099/Surgery, $p=0.0032$; Vehicle/Sham vs Vehicle/Surgery, $p<0.0001$; **Supplemental Figure 1b**). Thus, these results suggest that orthopedic surgery did not adversely affect the ability of mice to perform this task. No differences in total time spent exploring objects across each phase of the task was observed (**Supplemental Figure 1c**). Thus, we believe our data reflect differences in memory performance and not differences in locomotive behavior.

We further evaluated memory using a novel Memory Load Object Discrimination task (Sannino et al., 2012). In this modified novel object discrimination task, mice are presented with a single object during the first trial, and then additional objects are subsequently added to the testing arena for each subsequent trial until seven trials are completed (totaling seven objects for the final test trial) (**Figure 3c**). Each subsequent trial (beyond trial 2) tests the mouse’s ability to discriminate a novel object from *multiple* familiar objects, and therefore the task ultimately tests memory load. Using RMANOVA, we identified a significant main effect of treatment on memory preference score in this task [$F (3, 36) = 6.719$, $p = 0.001$]. Vehicle-treated mice that received surgery performed significantly worse overall relative vehicle-treated ($p = 0.003$) and URMC-099-treated ($p =0.0015$) sham controls (**Figure 3d**). Further, URMC-099 treatment prevented memory load impairment in mice receiving surgery ($p = 0.0025$) (**Figure 3d**). Taken together, the results from these two behavioral tasks implicate hippocampus-dependent impairments in episodic memory and memory load in our vehicle-treated surgery group that were prevented by prophylactic treatment with URMC-099.

URMC-099 pre-treatment does not alter bone fracture healing

A major concern regarding the use of anti-inflammatory drugs for PND is whether they will adversely affect non-cognitive endpoints, such as fracture healing. This is primarily because fracture healing depends on the early production of pro-inflammatory cytokines (Cho, Gerstenfeld, & Einhorn, 2002) and the recruitment of inflammatory cells that mediate distinct phases of fracture repair (Claes, Recknagel, & Ignatius, 2012). To evaluate whether prophylactic URMC-099 adversely affected bone healing, we harvested fracture calluses 21 days post fracture and used microCT and histomorphophometry analyses to quantify bone healing. MicroCT assessment demonstrated no difference in bone mineralization during fracture healing (**Figure 4a-c**) and histomorphometry analysis confirmed no difference in bone deposition (**Figure 4d-e**) in response to URMC-099 treatment. URMC-099 directly interferes with pro-inflammatory cytokine expression by inhibiting kinases that mediate this process (Goodfellow et al., 2013; Marker et al., 2013). Given our bone healing data, we conjecture that URMC099 does not completely abrogate inflammatory responses and may allow certain beneficial inflammatory processes to occur. In support of this notion, we have shown previously that URMC-099 does not fully inhibit HIV-1 Tat-induced pro-inflammatory cytokine expression in monocytes (Goodfellow et al., 2013) and microglia (Marker et al., 2013). It is alternatively possible that anti-inflammatory drugs that *do* interfere with bone healing, such as nonsteroidal anti-inflammatory drugs, mediate their detrimental effects through multiple mechanisms that extend beyond the initial mobilization of innate immunity, as has been suggested by others (Ramirez-Garcia-Luna et al., 2019). Finally, although MLK3 activation is known to regulate bone mineralization (Zou et al., 2011), we contend that our prophylactic, time-limited, treatment paradigm helped to preclude any detrimental effect of our drug on long-term bone repair.

In conclusion, the present study further defines the neurocognitive sequelae that accompany orthopedic surgery and highlights the therapeutic efficacy of URMC-099’s broad-spectrum activity in a mouse model of PND. In light of our recent findings that URMC-099 is therapeutically advantageous to a more highly-selective MLK3 inhibitor in experimental autoimmune encephalitis (Bellizzi et al., 2018), our data suggest that inhibiting multiple kinase signaling pathways in parallel or downstream from MLK3 is beneficial and may be necessary to effect disease-modifying outcomes.

Materials & Methods

Animals – All animal procedures were carried out under protocols approved by Duke University Medical Center and University of Rochester Medical Center, Institutional Animal Care and Use Committee within the National Research Council Guide for the Care and Use of Laboratory Animals, 8th edition. Both Duke University and Rochester Medical Center are AAALAC accredited institutions.

Orthopedic surgery model – Orthopedic surgery was performed as described previously (Xiong et al., 2018). Briefly, the left hind limb was subjected to an open tibial fracture with intramedullary fixation under general anesthesia (isoflurane: 4% induction, 2% maintenance) and analgesia (buprenorphine: 0.1 mg/kg s.c.). Sham treated mice were administered anesthesia and analgesia as above but without surgical intervention.

URMC-099 administration – URMC-099 (M.W. 421) was synthesized as originally described in Goodfellow et al. (Goodfellow et al., 2013). URMC-099 drug solutions were prepared by dissolving 20 mg of URMC-099 in 0.5 mL sterile dimethyl sulfoxide (DMSO; D8779, Sigma). We then added 4 mL polyethylene glycol 400 (PEG400; 91893-250-F, Sigma) and 5.5 mL sterile saline (Hospira National Drug Code NDC0409-4888-10), which yields 10 mL of 2 mg/mL URMC-099 drug solution. “Vehicle” solution refers to the same solution minus URMC-099. For the experiments described in Fig. 1, mice were injected i.p. with three doses prior to orthopedic surgery and two doses post-surgery, all spaced 12 hr apart. For all other experiments, mice were only treated prophylactically – i.e., with only 3 doses (spaced 12 hr apart) prior to surgery. Drug solutions were coded such that experimenters were blind to the experimental conditions for the duration of the experiment.

Piezoelectric thinned-skull cortical window surgery – The thinned skull cortical window (TSCW) procedure was performed using a piezoelectric surgical technique (Clark et al., 2018). Piezoelectric surgery was performed using a piezosurgery handpiece (Mectron) fitted with an OT11 osteotomy insert (Mectron) under constant, manual irrigation (1 mL/min) with ice-cold aCSF to minimize the heating of the bone during the thinning process. A cover glass was glued over the thinned area of skull and a custom head plate was placed with dental cement to facilitate repeated intravital imaging. Isoflurane was used for anesthesia (4% induction, 2% maintenance) during the TCSW procedure. The TCSW surgery was limited to 30 min or less to minimize the mouse’s exposure to variables that might confound this study’s results (e.g., duration under anesthesia).

Two-photon intravital microscopy – A custom two-photon laser-scanning microscope was used for intravital imaging (Ti:Sapphire, Mai-Tai, Spectraphysics; modified Fluoview confocal scan head, ×20 lens, 0.95 numerical aperture, Olympus). Two-photon excitation was achieved using 100-fs laser pulses (80MHz) tuned to 840nm with a power of ~50mW measured at the sample after the objective lens. For all experiments, a 565 nm dichroic mirror was used in conjunction with 580/180 (GFP) and 605/55 (rhodamine B) filters. Rhodamine B dextran (2% w/v, 75ul total) was injected retroorbitally after anesthetization with ketamine (100 mg/kg)/xylazine (10mg/kg) and 5 minutes prior to intravital imaging. Mice were maintained at 37^0C during intravital imaging and recovery. Importantly, intravital imaging sessions were limited to 40 minutes per mouse to avoid re-dosing with ketamine/xylazine. Intravital imaging was performed using 4X digital zoom and 512 x 512pixel resolution. Stacks containing 41 slices (1um step size) were imaged every 90 seconds for 15 minutes to obtain the XYZT stacks used for analysis.

CLARITY tissue processing and light-sheet microscopy – Brains were harvested following transcardial perfusion with 30 to 50 mL of PBS (Gibco, #10010-023) and 20 to 30 mL 4% paraformaldehyde (PFA) (Sigma, #158127) in PBS, pH 7.4, under isoflurane anesthesia. After a post-fixation step (24 h in 4% PFA at 4°C), brains were sectioned by vibratome into 1 mm-thick coronal sections. Sections were put in 1x PBS overnight at 4°C prior to polymerization and tissue clearing. Polymerization and tissue clearing were accomplished using the X-CLARITY™ reagents and equipment (Logos Biosystems). Sections were first saturated in 1mL hydrogel solution (X-CLARITY™ Hydrogel Solution Kit, #C1310X, Logos Biosystems) at 4°C for 24h and were subsequently incubated in the polymerization system for 3 h at 37°C. Polymerized

sections were then actively cleared in electrophoretic tissue clearing (ETC) solution (#C13001, Logos Biosystems) using the X-CLARITY™ Tissue Clearing System with the following settings: 0.9 A, 37°C, for 3h. Cleared sections were washed overnight three times with 0.2% triton-X100 (T8787, Sigma) in PBS on a shaker at room temperature. Immunohistochemistry was performed by incubating cleared tissue sections in primary antibody solutions containing primary antibodies (Rabbit anti-Iba1, cat no. 019-19741, Wako) in 10% normal donkey serum + 0.2% triton-X100 in PBS (blocking buffer) at 4°C for 3 days. Following three wash steps (0.1% triton-X100 in PBS, overnight at 4°C), sections were incubated with secondary antibodies and DAPI diluted in blocking buffer for 3 days at 4°C. Sections were subsequently stored in PBS until mounting.

For imaging, sections were mounted in 1% agarose (#BP160-100, FisherScientific) and hanged in 1mL syringes (#300013, BD Biosciences) without tips followed by incubated with mounting solution (#C13101, Logos Biosystems) at 4°C overnight. Samples were then moved to room temperature for 1 h before imaging. Imaging was performed using a light sheet fluorescence microscope (LSFM, Z1, Zeiss, Germany) at the Duke University Light Microscopy Core Facility. Imaging was performed by suspending samples with mounting solution in a CLARITY-optimized sample chamber and orienting the samples such that they were parallel to the detection lens. XYZ stacks were acquired at 1920 x 1920 pixel resolution and 16-bit depth using 5x or 20x objectives. The refractive index of the detection objective was set as 1.46. A 405/488/561/640 filter set was used for laser excitations with laser intensities set between 0.5 and 2%. An exposure time of 29.97 ms for each frame was used and a step size of 0.659 µm was used. Three-dimensional surface reconstructions of microglia were achieved using Imaris as described below.

Imaris Image Analysis – Individual microglia were cropped from XYZT stacks, registered, and drift-corrected using ImageJ. Individual microglia XYZT stacks were imported into Imaris (Bitplane) for analysis. For motility analysis, the “Spots” function was used to assign spots to individual microglial processes. Spots were assigned automatically using an estimated diameter of 2 microns, which were subsequently filtered by “Quality” and again manually to remove Spots that did not correspond to the individual microglia under analysis. The “Connected Components” algorithm was then used to generate the movement tracks that were quantified. Movement tracks with a duration of less than 3min were excluded from analysis. For morphological analysis, the “Surface” function was used. Surface detail was set to 0.691 microns. Surfaces were then generated by manual thresholding and manually filtered to exclude surfaces that did not correspond to the individual microglia under analyses. Sphericity, defined as the ratio of the area of a sphere (with the same volume as the given particle) to the surface area of the particle, was used to quantify microglial morphology. Similar measures have been used previously to quantify changes in microglia morphology, albeit in 2-dimensions (Madry et al., 2018). Three-dimensional surface reconstructions of microglia were also performed on XYZ stacks derived from CLARITY tissue sections using the “Surface” function as described above with the following modifications: individual microglia were not cropped (instead, whole XYZ stacks were reconstructed) and surface detail was set to 2 microns to facilitate image processing.

Behavioral Testing – Mice were all housed in a temperature and humidity controlled environment, in Optimice ventilated cages (Animal Care Systems, Centennial, CO) with free access to water and mouse chow (5R58 Mouse Pico Diet,LabDiet, St. Louis, MO) under a 14 hr light: 10 hr dark light cycle with the onset of light at 0700 hrs. For all behavioral tests, mice were moved to the test room immediately following surgery and remained in the test room for the duration of the study. All test rooms were maintained under the same conditions as the main housing room. Two memory tasks were administered to assess different aspects of memory performance 24 hours following orthopedic surgery. The first task, The Eichenbaum What-Where-When Object Recognition Test (DeVito & Eichenbaum, 2010) was used to evaluate different aspects of episodic memory. Mice were habituated to a 60 x 40 x 24 cm testing arena for 5 min. The testing portion of the task involves three trials designated “Set A”, “Set B”, and “Challenge.” In Set A, mice were returned to the testing arena to explore four identical Set A objects placed in configuration A (**Figure 3a**) for 5 min. Mice were returned to their cages for an inter-trial interval (ITI) of 50-55 min, after which they were returned to the arena now containing Set B objects in configuration B (**Figure 3a**) for 5 min. The Challenge trial was administered after a 50-55 min ITI and included two Set A and two B objects arranged in alternating sequence to “What”, “Where”, and “When” aspects of episodic memory (**Figure 3a**). The actual objects used are depicted in **Supplementary Figure 1a**. All behavioral

trials were recorded via a video camera suspended above the testing arena interfaced to a computer running Media Player II (Noldus Information Technology, Ashefille, NC). Videos were scored using behavioral recognition and nose-point tracking with Ethovision 11 (Noldus Information Technology, Asheville, NC). Variables scored included duration of contacts within each object zone (contact = nose within 1 cm of physical object with the body axis oriented toward the object). “What”, “Where”, and “When” memory indices were computed from exploration times in the Challenge trial. The “What” aspect of episodic memory was defined as the mean exploration time for both A objects minus the mean exploration time for both B objects over the mean exploration time of all objects and takes advantage of the animal exploring the less recently experienced objects (A objects) more than those recently experienced (B objects). The “Where” aspect was defined as the mean exploration time for displaced object A minus the mean exploration time for stationary object A over the mean exploration time of both A objects. The “When” aspect was defined as the mean exploration time for “oldest” stationary object A minus the mean exploration time for the two most recent B objects over the mean exploration time for all three of these objects. The “When” index takes advantage of mice exploring the less recent “A” object over the more recent “B” objects while these objects all remain in their original locations.

Memory load was evaluated using a novel Memory Load Object Discrimination test (Sannino et al., 2012). This task was performed in a 42 x 42 x 20 cm testing arena and consisted of seven trials (ranging from 2 to 5 min depending on the number of objects present) separated by an ITI of 1-2 min. On each subsequent trial, a unique, novel object was placed in the arena along with the previously presented objects (i.e. the “familiar” objects). Thus, the testing arena contained 1 object in trial 1, two objects in trial 2, three in trial 3, and so on. The actual objects used are depicted in **Supplemental Figure 2a**. Trial lengths were increased as the number of objects was increased, as follows: 2 min (trials 1-3), 3 min (trials 4-5), 5 min (trials 6-7). For each trial, the newly added object was designated the “target” object. Time spent exploring the target object versus all other objects was recorded as described above for the “What”-“Where”-“When” task. Memory preference scores for each trial were computed as ratios of the mean exploration time for the target object minus the mean exploration time for all other objects over the mean exploration time for all objects.

Analysis of Fracture Healing – Fracture calluses were assessed as previously described (Baht, Nadesan, Silkstone, & Alman, 2017). Samples were dissected 21 days after injury and fixed in 10% Zn-formalin at room temperature for 5 days. Micro-computed tomography (microCT) analysis was conducted using a Scanco vivaCT 80 (Scanco Medical, Brüttisellen, Switzerland) at a scan resolution of 8µm. Calluses were scanned 1mm proximal and 1mm distal from the fracture site and assessed for total volume (TV) and bone volume (BV) in mm^3, and bone mineral density (BMD) in mg HA/mm^3. Fixed fracture calluses were decalcified using 12% EDTA pH 7.4, cleared of EDTA, and embedded into paraffin. Sections were cut at a thickness of 5µm and stained using safranin-O/fast-green to visualize bone and cartilage. A minimum of five sections were used to conduct computer-assisted histomorphometry analysis and results were presented as an amount relative to the total area of the fracture callus.

Statistics – All data were analyzed by Graphpad PRISM (GraphPad Software, San Diego, CA) and represented as mean ± SEM. Bone healing data was analyzed by unpaired, two-tailed t-test. The rest of the data was analyzed by one-way or two-way (repeated-measures) ANOVA with Dunnett’s multiple comparison test as indicated in the text for each experiment. Statistical significance is defined as $p < 0.05$ throughout.

Figure Legends

Figure 1. URMC-099 treatment *reverses* microgliosis and blood brain barrier leak following orthopedic surgery. 9-month old male mice underwent open tibial fracture and were terminated 24hr surgery. URMC-099 was given i.p. at 10 mg/kg, 3 doses before surgery and two doses after surgery based on Marker et al. 2013. ***A,*** representative images of F4/80 microglial/macrophage staining (top panels) and IgG staining (bottom panels) show that URMC-099 significantly attenuated microgliosis activation in the hippocampus. **B**, Differences in microglia cell numbers were quantified by unbiased stereology. **C**, IgG relative optical density was quantified to measure differences in blood brain barrier opening. *P<0.05, ***P<0.001, one-way ANOVA with Dunnett's multiple comparison test. Bars represent mean ± S.E.M.

Figure 2. URMC-099 prophylaxis *prevents* microglial morphological changes following orthopedic surgery. 3-month old mice received three doses i.p. of URMC-099 (10 mg/kg) prior to undergoing sham or orthopedic surgery. **A**, Representative cropped and drift-corrected XYZ stacks obtained by 2PLSM (top panels), Imaris 3D surface reconstructions (middle panels), and process movement tracks (bottom panels) (scale bar = 10 μm). **B**, Orthopedic surgery increased microglial sphericity in vehicle-treated, but not URMC-099-treated, mice. No differences were observed for mean track speed, **C**, nor mean track length, **D**. **E**, Representative 3D surface reconstructions of light-sheet micrographs obtained from optically cleared hippocampal sections (scale bar = 500 μm, top panels; scale bar = 100 μm, bottom panels). **F**, Mean microglial sphericity was increased by orthopedic surgery and URMC099 treatment prevented this. *P<0.05, **P<0.01, repeated-measures ANOVA (B-D) or one-way ANOVA (F) with Dunnett's multiple comparison test. Bars represent mean ± S.E.M.

Figure 3. URMC-099 prophylaxis abrogates orthopedic surgery-induced memory deficits. 3-month old mice received three doses i.p. of URMC-099 (10 mg/kg) prior to undergoing sham or orthopedic surgery. **A**, Illustration of Memory Load Object Discrimination test. **B**, illustration of "Where-What-When" Object Discrimination test. **C**, URMC-099 prevented surgery-induced impairments in mean target preference. **D**, URMC-099 prevented surgery-induced impairments in the "Where" and "What" aspects of the WWW task. *P<0.05, **P<0.01, repeated-measures ANOVA with Dunnett's multiple comparison test. Bars represent mean ± S.E.M.

Figure 4. URMC-099 pre-treatment does not alter bone fracture healing. 3-month old male mice were treated with either URMC-099 or vehicle and fractures were induced surgically. Fracture calluses were investigated 21 days post fracture to assess bone healing. **A**, microCT was used to assess bone volume per total callus volume (**B**) and bone mineral density (**C**) (scale bar = 1 mm). **D**, histomorphometry was used to determine percent bone tissue within the fracture callus (**E**). Data analyzed by unpaired two-tailed t-test. Bars represent mean ± S.E.M.

Supplementary information

Supplementary Figure 1: **Orthopedic surgery does not impair mice's ability to perform the WWW task**. 3-month old mice received three doses i.p. of URMC-099 (10 mg/kg) prior to undergoing sham or orthopedic surgery. Behavioral tasks were administered beginning 24 hours post-surgery. **A**, Illustration depicting the arena and objects used for the task. **B**, Orthopedic surgery increased the total distance moved during "Set A" relative to sham-treated controls for both vehicle- ($p<0.0001$) and URMC-099-treated mice ($p<0.01$). **C**, Neither surgery nor drug treatment affected total exploration times throughout the task. Data analyzed by repeated-measures ANOVA with Tukey's multiple comparison test.

Supplementary Figure 2: **Exploration times for target versus average of other objects for the MLOD task.** 3-month old mice received three doses i.p. of URMC-099 (10 mg/kg) prior to undergoing sham or orthopedic surgery. Behavioral tasks were administered beginning 24 hours post-surgery. **A**, Illustration depicting the objects used for the task. **B**, Illustration indicating the mouse starting position for the test. **C**, Trial exploration times for each experimental condition.

Video S1

Video depicting the Imaris-based 3D surface rendering and motility measurement for an individual microglia from a vehicle-treated mouse before surgery.

Video S2

Video depicting the Imaris-based 3D surface rendering and motility measurement for an individual microglia from a vehicle-treated mouse after surgery.

Video S3

Video depicting the Imaris-based 3D surface rendering and motility measurement for an individual microglia from a URMC-099-treated mouse before surgery.

Video S4

Video depicting the Imaris-based 3D surface rendering and motility measurement for an individual microglia from a URMC-099-treated mouse after surgery.

Video S5

Video depicting Iba1 immunoreactivity in a 1 mm thick hippocampal section cleared using CLARITY from a sham-treated mouse.

Video S6

Video depicting Iba1 immunoreactivity in a 1 mm thick hippocampal section cleared using CLARITY from a vehicle-treated surgery mouse.

Video S7

Video depicting Iba1 immunoreactivity in a 1 mm thick hippocampal section cleared using CLARITY from a URMC-099-treated surgery mouse.

References:

Ags/Nia Delirium Conference Writing Group, Planning Committee, & Faculty. (2015). The American Geriatrics Society/National Institute on Aging Bedside-to-Bench Conference: Research Agenda on Delirium in Older Adults. *J Am Geriatr Soc, 63*(5), 843-852. doi:10.1111/jgs.13406

Baht, G. S., Nadesan, P., Silkstone, D., & Alman, B. A. (2017). Pharmacologically targeting beta-catenin for NF1 associated deficiencies in fracture repair. *Bone, 98*, 31-36. doi:10.1016/j.bone.2017.02.012

Bellizzi, M. J., Hammond, J. W., Li, H., Gantz Marker, M. A., Marker, D. F., Freeman, R. S., & Gelbard, H. A. (2018). The Mixed-Lineage Kinase Inhibitor URMC-099 Protects Hippocampal Synapses in Experimental Autoimmune Encephalomyelitis. *eNeuro, 5*(6). doi:10.1523/ENEURO.0245-18.2018

Cho, T. J., Gerstenfeld, L. C., & Einhorn, T. A. (2002). Differential temporal expression of members of the transforming growth factor beta superfamily during murine fracture healing. *J Bone Miner Res, 17*(3), 513-520. doi:10.1359/jbmr.2002.17.3.513

Cibelli, M., Fidalgo, A. R., Terrando, N., Ma, D., Monaco, C., Feldmann, M., . . . Maze, M. (2010). Role of interleukin-1beta in postoperative cognitive dysfunction. *Ann Neurol, 68*(3), 360-368. doi:10.1002/ana.22082

Claes, L., Recknagel, S., & Ignatius, A. (2012). Fracture healing under healthy and inflammatory conditions. *Nat Rev Rheumatol, 8*(3), 133-143. doi:10.1038/nrrheum.2012.1

Clark, S. D., Mikofsky, R., Lawson, J., & Sulzer, D. (2018). Piezo High Accuracy Surgical Osteal Removal (PHASOR): A Technique for Improved Cranial Window Surgery in Mice. *J Vis Exp*(133). doi:10.3791/56172

DeVito, L. M., & Eichenbaum, H. (2010). Distinct contributions of the hippocampus and medial prefrontal cortex to the "what-where-when" components of episodic-like memory in mice. *Behav Brain Res, 215*(2), 318-325. doi:10.1016/j.bbr.2009.09.014

Dong, W., Embury, C. M., Lu, Y., Whitmire, S. M., Dyavarshetty, B., Gelbard, H. A., . . . Kiyota, T. (2016). The mixed-lineage kinase 3 inhibitor URMC-099 facilitates microglial amyloid-beta degradation. *J Neuroinflammation, 13*(1), 184. doi:10.1186/s12974-016-0646-z

Evered, L., Silbert, B., Knopman, D. S., Scott, D. A., DeKosky, S. T., Rasmussen, L. S., . . . Nomenclature Consensus Working, Group. (2018). Recommendations for the nomenclature of cognitive change associated with anaesthesia and surgery-2018. *Br J Anaesth, 121*(5), 1005-1012. doi:10.1016/j.bja.2017.11.087

Feng, X., Valdearcos, M., Uchida, Y., Lutrin, D., Maze, M., & Koliwad, S. K. (2017). Microglia mediate postoperative hippocampal inflammation and cognitive decline in mice. *JCI Insight, 2*(7), e91229. doi:10.1172/jci.insight.91229

Forsberg, A., Cervenka, S., Jonsson Fagerlund, M., Rasmussen, L. S., Zetterberg, H., Erlandsson Harris, H., . . . Eriksson, L. I. (2017). The immune response of the human brain to abdominal surgery. *Ann Neurol, 81*(4), 572-582. doi:10.1002/ana.24909

Goodfellow, V. S., Loweth, C. J., Ravula, S. B., Wiemann, T., Nguyen, T., Xu, Y., . . . Gelbard, H. A. (2013). Discovery, synthesis, and characterization of an orally bioavailable, brain penetrant inhibitor of mixed lineage kinase 3. *J Med Chem, 56*(20), 8032-8048. doi:10.1021/jm401094t

Gyoneva, S., Davalos, D., Biswas, D., Swanger, S. A., Garnier-Amblard, E., Loth, F., . . . Traynelis, S. F. (2014). Systemic inflammation regulates microglial responses to tissue damage in vivo. *Glia, 62*(8), 1345-1360. doi:10.1002/glia.22686

Kiyota, T., Machhi, J., Lu, Y., Dyavarshetty, B., Nemati, M., Zhang, G., . . . Gendelman, H. E. (2018). URMC-099 facilitates amyloid-beta clearance in a murine model of Alzheimer's disease. *J Neuroinflammation, 15*(1), 137. doi:10.1186/s12974-018-1172-y

Kondo, S., Kohsaka, S., & Okabe, S. (2011). Long-term changes of spine dynamics and microglia after transient peripheral immune response triggered by LPS in vivo. *Mol Brain, 4*, 27. doi:10.1186/1756-6606-4-27

Lee, H. B., Oldham, M. A., Sieber, F. E., & Oh, E. S. (2017). Impact of Delirium After Hip Fracture Surgery on One-Year Mortality in Patients With or Without Dementia: A Case of Effect Modification. *Am J Geriatr Psychiatry, 25*(3), 308-315. doi:10.1016/j.jagp.2016.10.008

Leslie, D. L., Marcantonio, E. R., Zhang, Y., Leo-Summers, L., & Inouye, S. K. (2008). One-year health care costs associated with delirium in the elderly population. *Arch Intern Med, 168*(1), 27-32. doi:10.1001/archinternmed.2007.4

Madry, C., Kyrargyri, V., Arancibia-Carcamo, I. L., Jolivet, R., Kohsaka, S., Bryan, R. M., & Attwell, D. (2018). Microglial Ramification, Surveillance, and Interleukin-1beta Release Are Regulated by the Two-Pore Domain K(+) Channel THIK-1. *Neuron, 97*(2), 299-312 e296. doi:10.1016/j.neuron.2017.12.002

Marker, Daniel F., Tremblay, Marie-Ève, Puccini, Jenna M., Barbieri, Justin, Gantz Marker, Mary A., Loweth, Colin J., . . . Gelbard, Harris A. (2013). The new small-molecule mixed-lineage kinase 3 inhibitor URMC-099 is neuroprotective and anti-inflammatory in models of human immunodeficiency virus-associated neurocognitive disorders. *The Journal of neuroscience : the official journal of the Society for Neuroscience, 33*(24), 9998-10010.

Paris, I., Savage, J. C., Escobar, L., Abiega, O., Gagnon, S., Hui, C. W., . . . Valero, J. (2018). ProMoIJ: A new tool for automatic three-dimensional analysis of microglial process motility. *Glia, 66*(4), 828-845. doi:10.1002/glia.23287

Ramirez-Garcia-Luna, J. L., Wong, T. H., Chan, D., Al-Saran, Y., Awlia, A., Abou-Rjeili, M., . . . Martineau, P. A. (2019). Defective bone repair in diclofenac treated C57Bl6 mice with and without lipopolysaccharide induced systemic inflammation. *J Cell Physiol, 234*(3), 3078-3087. doi:10.1002/jcp.27128

Sannino, S., Russo, F., Torromino, G., Pendolino, V., Calabresi, P., & De Leonibus, E. (2012). Role of the dorsal hippocampus in object memory load. *Learn Mem, 19*(5), 211-218. doi:10.1101/lm.025213.111

Terrando, N., Eriksson, L. I., Ryu, J. K., Yang, T., Monaco, C., Feldmann, M., . . . Maze, M. (2011). Resolving postoperative neuroinflammation and cognitive decline. *Ann Neurol, 70*(6), 986-995. doi:10.1002/ana.22664

Terrando, N., Gomez-Galan, M., Yang, T., Carlstrom, M., Gustavsson, D., Harding, R. E., . . . Eriksson, L. I. (2013). Aspirin-triggered resolvin D1 prevents surgery-induced cognitive decline. *FASEB J, 27*(9), 3564-3571. doi:10.1096/fj.13-230276

Terrando, N., Monaco, C., Ma, D., Foxwell, B. M., Feldmann, M., & Maze, M. (2010). Tumor necrosis factor-alpha triggers a cytokine cascade yielding postoperative cognitive decline. *Proc Natl Acad Sci U S A, 107*(47), 20518-20522. doi:10.1073/pnas.1014557107

Witlox, J., Slor, C. J., Jansen, R. W., Kalisvaart, K. J., van Stijn, M. F., Houdijk, A. P., . . . de Jonghe, J. F. (2013). The neuropsychological sequelae of delirium in elderly patients with hip fracture three months after hospital discharge. *Int Psychogeriatr, 25*(9), 1521-1531. doi:10.1017/S1041610213000574

Xiong, C., Zhang, Z., Baht, G. S., & Terrando, N. (2018). A Mouse Model of Orthopedic Surgery to Study Postoperative Cognitive Dysfunction and Tissue Regeneration. *J Vis Exp*(132). doi:10.3791/56701

Zhang, M. D., Barde, S., Yang, T., Lei, B., Eriksson, L. I., Mathew, J. P., . . . Terrando, N. (2016). Orthopedic surgery modulates neuropeptides and BDNF expression at the spinal and hippocampal levels. *Proc Natl Acad Sci U S A, 113*(43), E6686-E6695. doi:10.1073/pnas.1614017113

Zou, W., Greenblatt, M. B., Shim, J. H., Kant, S., Zhai, B., Lotinun, S., . . . Glimcher, L. H. (2011). MLK3 regulates bone development downstream of the faciogenital dysplasia protein FGD1 in mice. *J Clin Invest, 121*(11), 4383-4392. doi:10.1172/JCI59041

Figure 1

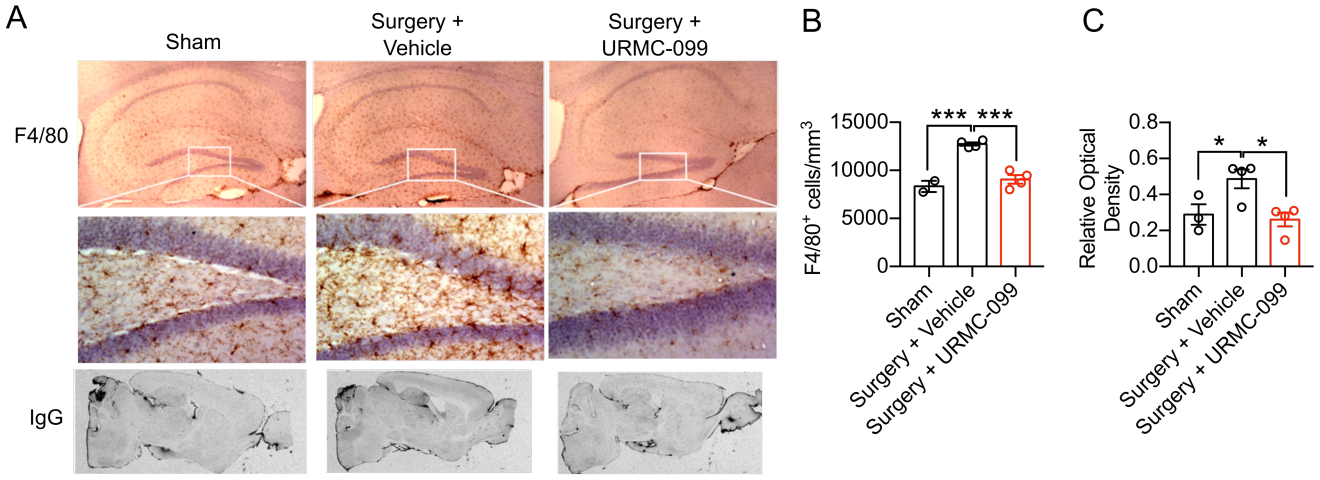
A
Sham
Surgery + Vehicle
Surgery + URMC-099
F4/80
IgG
B
F4/80+ cells/mm3
15000
10000
5000
0
***
***
Sham
Surgery + Vehicle
Surgery + URMC-099
C
Relative Optical Density
0.8
0.6
0.4
0.2
0.0
*
*
Sham
Surgery + Vehicle
Surgery + URMC-099

Figure 2

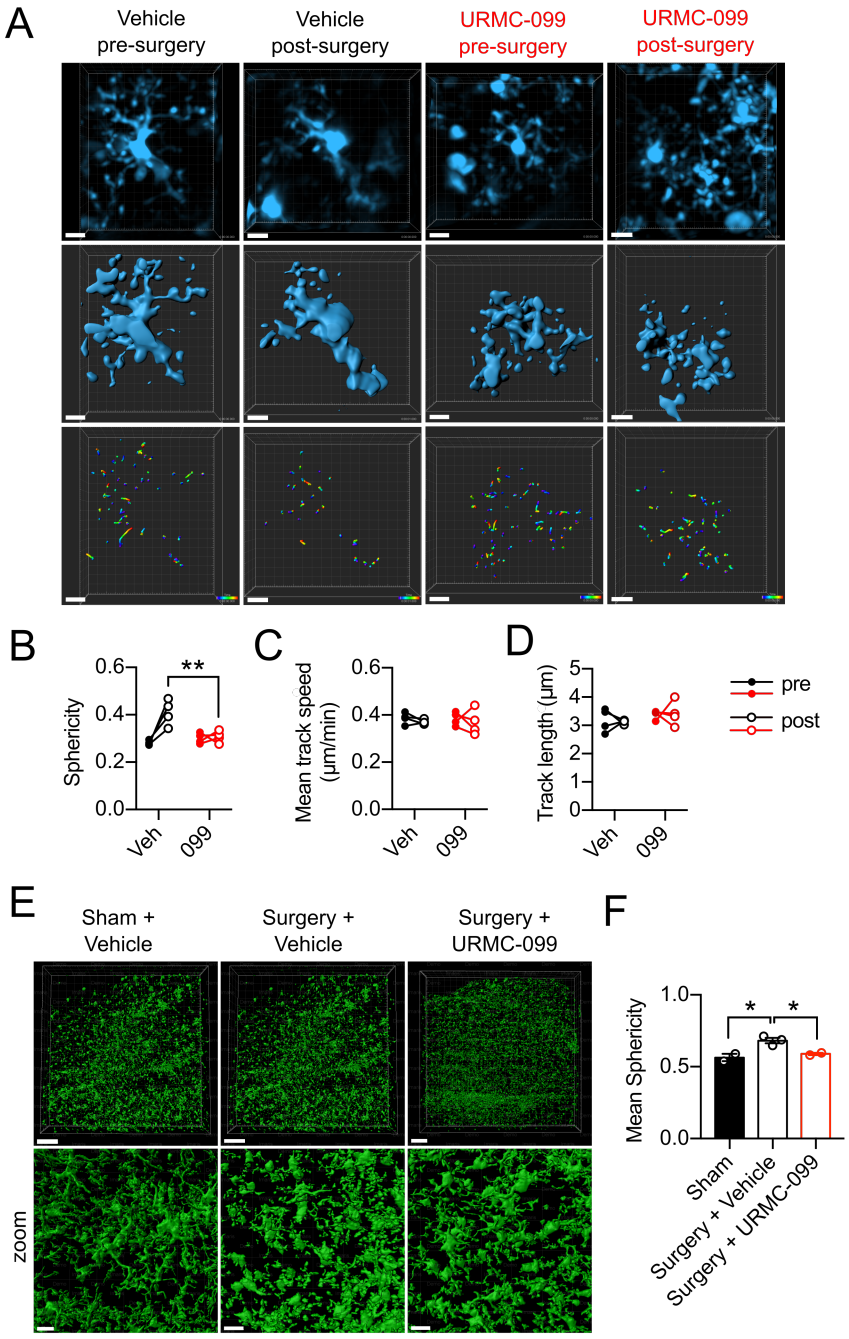
A
Vehicle pre-surgery
Vehicle post-surgery
URMC-099 pre-surgery
URMC-099 post-surgery
B
Sphericity
0.6
0.4
0.2
0.0
**
Veh
099
C
Mean track speed (µm/min)
0.6
0.4
0.2
0.0
Veh
099
D
Track length (µm)
5
4
3
2
1
0
Veh
099
pre
post
E
Sham + Vehicle
Surgery + Vehicle
Surgery + URMC-099
zoom
F
Mean Sphericity
1.0
0.5
0.0
*
*
Sham
Surgery + Vehicle
Surgery + URMC-099

Figure 3

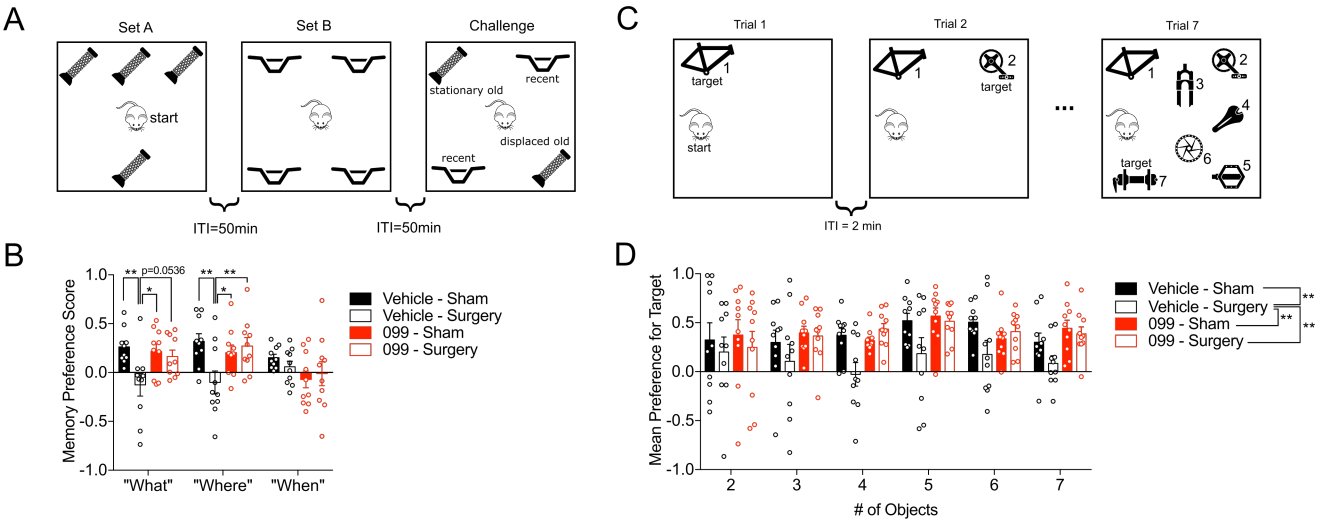
A
Set A
Set B
Challenge
start
stationary old
recent
displaced old
recent
ITI=50min
ITI=50min
B
Memory Preference Score
1.0
0.5
0.0
-0.5
-1.0
** p=0.0536
*
** **
*
"What"
"Where"
"When"
Vehicle - Sham
Vehicle - Surgery
099 - Sham
099 - Surgery
C
Trial 1
Trial 2
Trial 7
target
start
target
target
ITI = 2 min
D
Mean Preference for Target
1.0
0.5
0.0
-0.5
-1.0
2
3
4
5
6
7
# of Objects
Vehicle - Sham
Vehicle - Surgery
099 - Sham
099 - Surgery
**
**
**

Figure 4

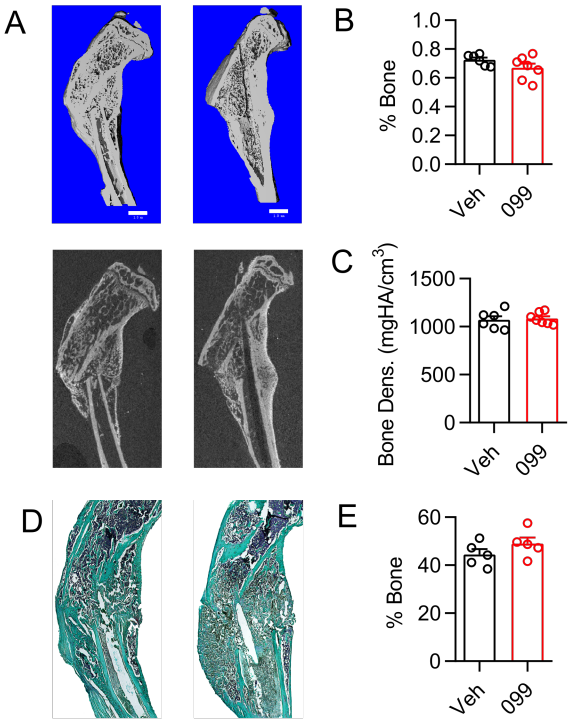
A
B
% Bone
1.0
0.8
0.6
0.4
0.2
0.0
Veh
099
C
Bone Dens. (mgHA/cm3)
1500
1000
500
0
Veh
099
D
E
% Bone
60
40
20
0
Veh
099